Surgical and Radiologic Anatomy (2019) 41:161–168
https://doi.org/10.1007/s00276-018-2136-8

ORIGINAL ARTICLE

The pterygopalatine fossa: morphometric CT study with clinical implications

Aleksandra Vuksanovic-Bozaric[1] · Batric Vukcevic[1] · Marija Abramovic[1] · Nemanja Vukcevic[1] · Natasa Popovic[1] · Miroslav Radunovic[1]

Received: 29 June 2018 / Accepted: 16 November 2018 / Published online: 23 November 2018
© Springer-Verlag France SAS, part of Springer Nature 2018

Abstract

Purpose The pterygopalatine fossa is a deep viscerocranial space containing the maxillary artery and nerve, the pterygopalatine ganglion, and the nerve of the pterygoid canal (vidian nerve). The endoscopic approach to this area relies on adequate preoperative imaging, such as computed tomography (CT). The aim was to determine the morphometric characteristics of the pterygopalatine fossa and its communications, including several previously unpublished measurements.

Methods 100 CT scans (56 male and 44 female patients) were analyzed. The axial, coronal, and sagittal slices, together with the three-dimensional reconstructions, were used in the study.

Results The central diameter and the length of the foramen rotundum, the vertical diameter and the length of the pterygoid (vidian) canal, and the diameter of the sphenopalatine foramen were significantly larger in men. The central diameters of the foramen rotundum and the vidian canal were significantly smaller than their anterior and posterior transverse diameters. The vidian canal length of 12.1 mm indicates the presence of the type 3 VC with a sensitivity of 83% and a specificity of 85%.

Conclusion Several new descriptions of the pterygopalatine fossa are presented here (such as the angle between the sphenopalatine foramen and the vidian canal, a new aspect in the understanding of the FR, and the distance between the posterior wall of the maxillary sinus to the vidian canal and the foramen rotundum), which might prove useful in the comprehension of the anatomy of the pterygopalatine fossa.

Keywords Computed tomography · Morphometry · Pterygopalatine fossa · Pterygoid canal

Introduction

The pterygopalatine fossa (PPF) is a deep space of the viscerocranium, located in front of the pterygoid process of the sphenoid bone, lateral to the perpendicular plate of the palatine bone, and posterior to the maxilla. Laterally, the PPF communicates with the infratemporal fossa through the pterygomaxillary fissure (PMF) [12]. The nasal cavity and the PPF communicate through the sphenopalatine foramen (SPF), located between the orbital and the sphenoidal process of the palatine bone. The inferior orbital fissure connects the PPF to the orbit. Posteriorly, the PPF communicates with the middle cranial fossa through the foramen rotundum (FR), and with the foramen lacerum through the pterygoid—vidian canal (VC) [27, 32, 33]. Acar et al. suggested a new VC classification based on its localization: type 1 (the VC is located inside the roof of the PPF), type 2 (the VC partially protrudes into the sphenoid sinus), and type 3 (the VC totally protrudes into the sphenoid sinus, with a stalk connecting it to the PPF roof) [1]. The palatovaginal canal represents a communication between the PPF and the nasopharynx [26], and the palatine foramina (the greater and the lesser) represents a communication between the PPF and the oral cavity [10]. The greater palatine foramen leads into the greater palatine canal (GPC), an inferior extension of the PPF [34].

Chen et al. [6] proposed a topographical division of the PPF into five parts: the GPC (from the hard palate to the PPF), the infrapterygopalatine segment of the PPF (from the PMF to the pterygopalatine ganglion), the pterygopalatine—ganglionic segment (in the level of the ganglion), and the suprapterygopalatine segment (from the pterygopalatine ganglion to the superior border of the FR, containing the

✉ Batric Vukcevic
batricvukcevic@gmail.com

[1] Faculty of Medicine, University of Montenegro, 20000 Podgorica, Montenegro

SPF, the FR, the VC, and the palatovaginal canal) and the roof of the PPF.

The clinical significance of the PPF lies in its numerous communications with the surrounding spaces, as well as the structures located in it: the maxillary artery and nerve, the pterygopalatine ganglion, and the nerve of the pterygoid canal (vidian nerve) [15, 29, 31]. The normal anatomy of the PPF may be changed due to various expansive or inflammatory lesions. The bony structures of the PPF and the infratemporal fossa are used as landmarks in the diagnosis and treatment of different pathological processes affecting the soft tissues of the face [30]. Therefore, the preoperative approach in the surgical management of viscerocranial disease includes modern imaging techniques such as computed tomography (CT), to provide adequate comprehension of the patient's facial skeleton.

The aim of the study was to determine the morphometric characteristics of the PPF and its communications, with several measurements that were not published previously. The results of the study may influence the surgery of the PPF, especially the endoscopic approach.

Materials and methods

A retrospective study on 100 patients' (56 male and 44 female; age range 33–62) CT scans was performed. Cases of facial fractures or skeletal disruptions, previous maxillofacial surgery, sinonasal tumors, or inflammatory conditions were excluded from the study to evaluate normal anatomy. In addition, cases with pneumatized pterygoid processes or pneumatized posterior wall of the maxillary sinus (MS) were not analyzed. SOMATOM Sensation 64 multi-slice scanner (Siemens Healthcare, Erlangen, Germany) was used to scan all the patients, with the following scanning protocol: exposure 120 kV, mAs 380, rotation time 1 s, pitch 0.85, slice thickness 1 mm, and interval 1 mm. The images were analyzed as native scans, as well as multiplanar and volume rendering technique reconstructions in sharp algorithm, using syngo fastView software on a dedicated workstation. Two observers (M.A. and B.V.) measured all the structures independently. Every measurement was taken three times, with the mean value used for the further analysis. The intraclass correlation ranged from 0.8 to 0.9 for all the measurements.

The axial slices (Fig. 1) were used to analyze the suprapterygopalatine segment of the PPF according to Chen et al. [6]. The slices displaying the maximum diameter and the total length of the FR, the VC, and the SPF were used to take the following measurements:

1. the transverse diameter of the FR and the VC at three levels: their anterior opening, central segment, and the posterior opening (Fig. 1a: 1, 2, and 3; Fig. 1b: 6, 7, and 8, for the FR and the VC, respectively)
2. the length of the FR (Fig. 1a: 4) and the VC (Fig. 1b: 9)
3. the transverse diameter of the SPF and the PMF (at the level of the VC) (Fig. 1b: 10 and 11, respectively)

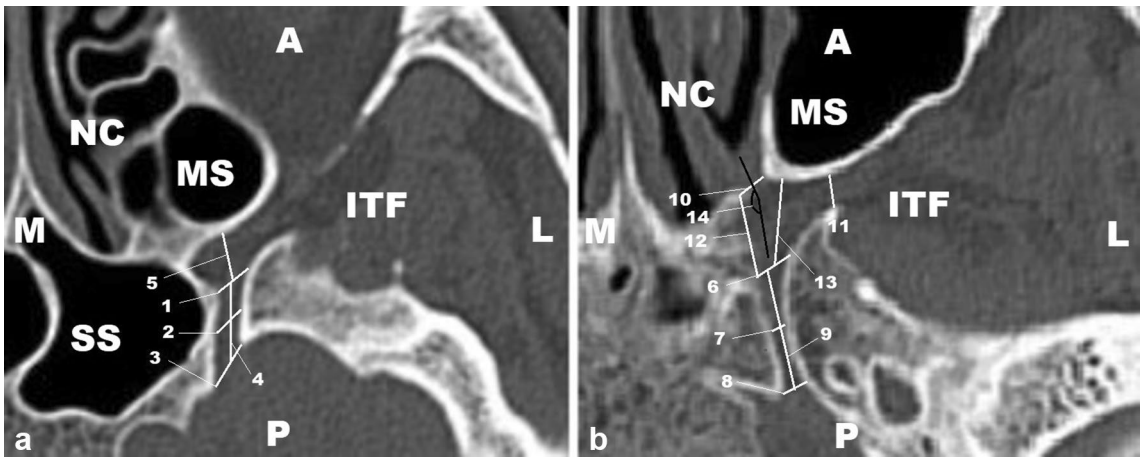

Fig. 1 Axial slices of the right pterygopalatine fossa used in measuring the vidian canal, the foramen rotundum, and the sphenopalatine foramen (the left pterygopalatine fossa). *A* anterior, *P* posterior, *M* medial, *L* lateral, *MS* maxillary sinus, *ITF* infratemporal fossa, *SS* sphenoid sinus, *NC* nasal cavity. **a** Level of the foramen rotundum; with 1, 2, and 3 representing its anterior, central, and posterior diameter, respectively. 4 The length of the foramen rotundum. 5 The distance from the posterior wall of the maxillary sinus to the foramen rotundum. **b** The level of the vidian canal. 6, 7, 8 The diameter of its anterior, central, and posterior segment, respectively. 9 The length of the vidian canal. 10, 11 The transverse diameter of the sphenopalatine foramen and the pterygomaxillary fissure, respectively. 12 The distance between the medial border of the anterior opening of the vidian canal to the posterior boundary of the sphenopalatine foramen. 13 The distance from the posterior wall of the maxillary sinus to the vidian canal. 14 The angle between the axis of the sphenopalatine foramen to the vidian canal

4. the direct distance between the medial boundary of the anterior opening of the VC to the posterior margin of the SPF (Fig. 1b: 12)
5. the direct distance between the posterior wall of the MS to the anterior opening of the FR (Fig. 1a: 5) and the VC (Fig. 1b: 13)
6. the angle between the SPF axis (a line perpendicular to the SPF) and the VC axis (Fig. 1b: 14).

The coronal slice depicting the maximum diameter of the VC and the FR was used to measure the direct distance from the FR and the VC to the midline (located at the level of the sphenoidal rostrum) (Fig. 2a: 1 and 2, respectively), as well as direct distance between the FR and the VC. Furthermore, the coronal slices were used to evaluate the VC type according to Acar et al. [1] (Fig. 2a). The sagittal slice showing the complete "inverted pyramid" shape of the PPF was used to measure its vertical diameter [the distance from the roof of the PPF to the superior opening of the GPC (Fig. 2b: 3)]. The 3D reconstruction of the posterior wall of the PPF was used to confirm the direct distance between the VC and the FR (Fig. 3: 3), as well as to measure the vertical diameters of their anterior openings (Fig. 3: 1 and 2, respectively). There was no significant difference between the values of the direct FR-VC distance measurement from the coronal slices and the 3D reconstructions. Owing to the fact that the anterior openings of the FR and the VC are not always exactly circular, a decision was made to measure the distance between their uppermost and lowermost points as their vertical diameters. Unfortunately, the palatovaginal canal was not measured because of frequent artifacts in its region, most likely due to technical issues.

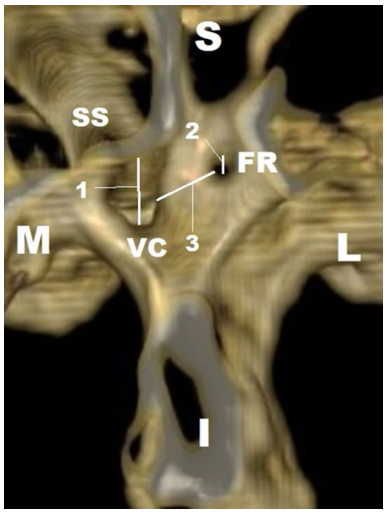

Fig. 3 The three-dimensional image used in the study (depicting the left pterygoid process), with 1 and 2 representing the vertical diameter of the anterior openings of the vidian canal (VC) and the foramen rotundum (FR), respectively; 3 as the direct distance between the aforementioned openings. *S* superior, *I* inferior, *M* medial, *L* lateral, *SS* sphenoid sinus

The standard statistical protocol for descriptive statistics was used, including the Shapiro–Wilk and the Kolmogorov–Smirnov tests for normality of distribution; the Levene test for homogeneity of variance; Student's *t* test for independent samples, ANOVA, and the Chi-squared test. The receiver-operating characteristic curve (ROC) was used to determine the cut-off value of the VC length useful in the prediction of the type 3 VC. A p value < 0.05 was considered statistically significant.

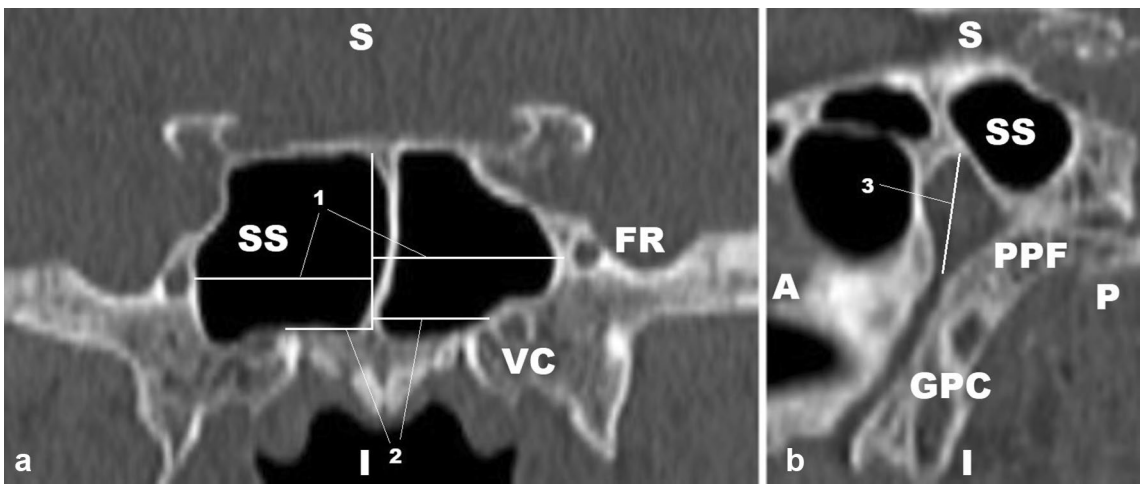

Fig. 2 The coronal (**a**) and the sagittal (**b**) slices of the sphenoid sinus (SS) utilized in the study, with 1 and 2 representing the distance from the midline to the foramen rotundum (FR) and the vidian canal (VC), respectively; 3 representing the vertical diameter of the pterygopalatine fossa (PPF). *S* superior, *I* inferior, *A* anterior; *P* posterior, *GPC* greater palatine canal

Results

All the results were distributed normally (according to the Shapiro–Wilk and the Kolmogorov–Smirnov test) and were homogeneous (as proven by the Levene test). The measures of the right and the left side failed to show a significant difference. This conclusion was reached both in male and in female patients.

Table 1 contains the measurements of the communications of the PPF. The central diameter of the FR was significantly larger in male compared to female patients ($p < 0.01$ on the right and $p = 0.012$ on the left side). A similar conclusion was reached in the comparison of the male and female FR length ($p = 0.039$ and $p = 0.015$ for the right side and the left side, respectively). Furthermore, there was a significant difference in the vertical diameter and the length of the VC, as well as the diameter of the SPF. These measurements were bilaterally larger in men ($p < 0.01$). The other measurements given in Table 1 did not show any significant difference between sexes.

ANOVA showed a significant difference among the transverse diameters of the anterior, central, and posterior segments of the FR bilaterally in both sexes ($p < 0.01$). The posterior diameter was the largest, followed by the anterior and the central diameter. In addition, the central diameter of the VC was significantly smaller than its anterior and posterior transverse diameters ($p < 0.01$). The difference between the anterior and the posterior diameter of the VC was not statistically significant ($p = 0.98$ on the right and $p = 0.64$ on the left side).

The measurements of various distances in the PPF are given in Table 2. The male patients showed a significantly larger angle between the SPF and the VC ($p = 0.014$ and

Table 1 The results of the diameters' measurements in the pterygopalatine fossa

	Male		Female	
	Right	Left	Right	Left
Transverse diameter of FR				
Anterior	3.8–6.7 (4.5 ± 0.6)	3.6–6.6 (4.3 ± 0.6)	3.7–6.3 (4.6 ± 0.6)	3.3–6.6 (4.5 ± 0.7)
Central	1.3–2.5 (1.6 ± 0.3)	1.2–2.5 (1.6 ± 0.3)	1–2.2 (1.4 ± 0.3)	1.1–2 (1.5 ± 0.2)
Posterior	4.0–6.9 (5.3 ± 0.6)	4.2–7 (5.3 ± 0.6)	4–6.8 (5.2 ± 0.6)	4.1–6.3 (5.1 ± 0.5)
Vertical diameter of FR	1.6–2.8 (2.1 ± 0.3)	1.5–2.7 (2.1 ± 0.3)	1.6–2.8 (2 ± 0.3)	1.5–2.5 (2 ± 0.2)
FR length	9–17.5 (12.2 ± 2.2)	7.5–1.6 (11.2 ± 2.1)	8–17.5 (12.1 ± 2.3)	7.5–17 (11 ± 2.1)
Transverse diameter of VC				
Anterior	2.4–4.9 (3.6 ± 0.5)	2–3.9 (3.6 ± 0.6)	1.9–4.8 (3.6 ± 0.5)	1.9–4.7 (3.5 ± 0.5)
Central	1.1–3.1 (2 ± 0.4)	1.1–3 (2 ± 0.4)	1.3–3 (2 ± 0.5)	2.3–2.9 (2 ± 0.4)
Posterior	2.1–5.6 (3.6 ± 0.7)	2.1–5.5 (3.6 ± 0.7)	2.0–5.4 (3.6 ± 0.6)	2–5.4 (3.6 ± 0.7)
Vertical diameter of VC	2.1–3.3 (2.6 ± 0.3)	2.2–3.3 (2.7 ± 0.3)	1.8–3 (2.5 ± 0.3)	1.8–3.2 (2.5 ± 0.4)
VC length	9–13 (11.9 ± 0.9)	9.2–13.6 (12 ± 1)	8.7–12.5 (11.1 ± 1)	8.9–12.4 (10.7 ± 0.8)
Transverse diameter of SPF	3.5–7.8 (5 ± 0.9)	3.4–7.4 (5.1 ± 0.9)	3.2–5.6 (4.4 ± 0.6)	3.2–5.5 (4.3 ± 0.6)
Transverse diameter of PMF	4.3–7.1 (5.1 ± 0.5)	4–7 (5.1 ± 0.6)	3.8–6.9 (4.9 ± 0.6)	4–6.9 (4.8 ± 0.6)

The range of values is given, with the mean value ± standard deviation in parentheses. All measurements are given in millimeters

Table 2 The results of various distances' measurements in the pterygopalatine fossa

	Male		Female	
	Right	Left	Right	Left
FR-to-VC distance (mm)	3.6–7.9 (5.1 ± 0.8)	3.5–7.9 (5.1 ± 0.9)	3.4–7.8 (5 ± 0.9)	3.5–7.7 (5.2 ± 1.1)
SPF-to-VC distance (mm)	5.9–8.3 (6.9 ± 0.4)	5.8–8.3 (6.8 ± 0.4)	5.6–7.8 (6.7 ± 0.5)	5.–7.9 (6.8 ± 0.4)
MS-to-VC distance (mm)	6.1–9.2 (8.3 ± 0.6)	6–9 (8.3 ± 0.6)	6.2–9 (8.3 ± 0.7)	6.2–9 (8.2 ± 0.6)
MS-to-FR distance (mm)	4.4–8.3 (6.3 ± 0.8)	4.4–8.5 (6.3 ± 0.7)	4.5–8.3 (6.4 ± 0.8)	4.8–8 (6.3 ± 0.6)
SPF-to-VC angle (degrees)	125.3–163.3 (148.4 ± 6.7)	122–162 (147.1 ± 7.3)	120–162 (144.2 ± 10.1)	119–162 (143 ± 9.8)
FR-to-midline distance (mm)	18.9– 28.7 (23.5 ± 1.9)	17.9– 29 (22.6 ± 2.8)	18.5– 26 (22.8 ± 2.2)	18.3– 26 (21.9 ± 2.6)
VC-to-midline distance (mm)	9.9– 17.1 (13.8 ± 1.4)	10.1–17.2 (13.7 ± 1.6)	9.7–16 (13.4 ± 1.4)	9.6–16.5 (13.1 ± 1.7)
Vertical diameter of PPF	14.5–22.5 (18.5 ± 1.8)	14.8–21.5 (18.4 ± 1.7)	14.1–21.8 (17.8 ± 2)	13.9–20 (18.1 ± 1.5)

The range of values is given, with the mean value ± standard deviation in parentheses. All measurements are given in millimeters

$p = 0.02$ for the right side and the left side, respectively), as well as the distance from the VC to the midline on the left side ($p = 0.032$). The distance from the MS to the VC was significantly greater than the distance from the MS to the FR in both sexes bilaterally ($p < 0.01$).

Table 3 contains the occurrence of different VC types in the analyzed material. The Chi-squared test failed to show a significant difference in the comparison of the two sides, as well as the two sexes. The VC types are shown in Fig. 4.

An ROC curve was computed to determine the value of VC length as the cut-off value for the type 3 VC. The VC length of 12.1 mm indicates the presence of the type 3 VC with a sensitivity of 83% and a specificity of 85%, with an area under the curve (AUC) of 0.74.

Discussion

Several previously unpublished measurements are reported here (such as the angle between the SPF and the VC, as well as the distance from the MS to the VC and the FR), with the intent to further illustrate the relations of different structures in the PPF. The distance between the SPF and the VC (average value of 6.8 mm) and the angle between the SPF and the VC (average value of 145.7°) may illustrate a possible endoscopic access to the PPF and the VC through the SPF. The difference in the distance from the MS to the VC and the FR shows the medial widening of the PPF. Hypothetically, the transmaxillary approach would show that it is easier to access the FR than the VC. In addition, to prevent iatrogenic injury to the maxillary nerve, the proximity of the FR to the MS must be appreciated.

Table 3 The types of the vidian canal (VC) according to Acar et al. [1] by percentage

	Male		Female	
	Right	Left	Right	Left
VC type (%)				
Type 1	61	60	59	60
Type 2	32	34	35	33
Type 3	7	6	6	7
Total (%)	100	100	100	100

Type 1 the VC is located inside the roof of the PPF. *Type 2* the VC partially protrudes into the sphenoid sinus. *Type 3* the VC totally protrudes into the sphenoid sinus

The average VC length of 11.4 mm is similar to the value reported by Acar et al. [1]: 12.9 ± 1.9 mm. The cut-off value of 12.1 mm strongly predicts the existence of type 3 VC (total protrusion of the canal into the sphenoid sinus). This result may prove useful in the transsphenoidal approach to the VC, with a conclusion that the canals protruding into the sinus are usually longer than 12.1 mm. It is understandable that, in the era of modern radiologic techniques, the VC length does not have to be predicted—since a coronal CT scan is necessary in all patients undergoing endoscopic sinus surgery. However, the observation presented here may spark interest in future research—whether the vidian nerve is also significantly longer in VC type 3 and what are the neurological and surgical implications of that anatomical feature.

Acar et al. [1] performed a CT study on 250 patients, reporting the type 1 VC in 55.6% patients, the type 2 in 34.8%, and the type 3 in 9.6%, in accordance with the results presented herein. On the other hand, Mohebbi et al. [24] reported the VC to be located inside the sphenoid sinus in 28% of cases, with 48% of cases showing partial protrusion of the canal, and 24% having the VC completely inside the roof of the PPF. Of all the cases analyzed by Mohebbi et al., 54% showed pneumatized pterygoid processes, which possibly increased the occurrence of VC protrusion into the sphenoid sinus, by extending the sinus inferiorly into the root of the pterygoid process. The subsequent research should take into account various types of sphenoid sinus pneumatization (as described by Rusu et al. [30]) to analyze their potential influence on the anatomy of PPF communications.

Daniels et al. [9] proved a description of the FR as a "sagitally oriented channel", which appreciates the FR as a canal with a certain length. The approach to the FR measurement employed here sheds a new light on the understanding

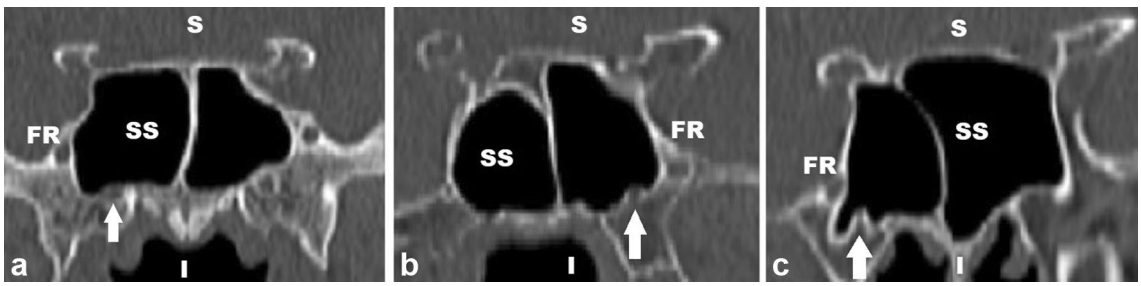

Fig. 4 The three types of the vidian canal as observed in the study. **a** represents type (1); **b** represents type (2); **c** represents type (3). The arrows indicate the vidian canals. *S* superior, *I* inferior, *SS* sphenoid sinus, *FR* foramen rotundum

of the FR. The FR is here viewed as a canal measuring 11.6 mm in average length, and with a narrow central segment. Decompression of the maxillary nerve inside the FR requires the narrowing of the FR to be comprehended. In 2011, Rusu described a previously unreported doubled foramen rotundum (associated with maxillary nerve fenestration) [28], a variation which was not observed in this research.

The results of the PPF measurement published in the relevant literature are given in Table 4. Despite its level of detail, the study conducted by Chen et al. [6] has to be addressed with the possibility of individual morphometric variation due to the small sample size. It is noted that Chen et al. [4], Kim et al. [6], and Berlis et al. [22] did not inform of the level of the FR's transverse diameter measurement, and therefore, their results cannot be directly compared to the results published herein. The direct distance between the FR and the VC reported by Mohebbi et al. might have been influenced by the occurrence of pterygoid process pneumatization in their study sample, as already described [24]. Acar et al. also analyzed a significant number of cases with pterygoid process pneumatization (39.2% of the total sample), which might have influenced the aforementioned distance to be larger [1]. In the study presented herein, pterygoid process pneumatization was taken an exclusion criteria to prevent extreme values of the direct distance between the FR and the VC. The 3D CT study by Hwang et al. lacks the details regarding the level of the VC and the FR measurement. The authors analyzed the anterior aspect of the pterygoid process, meaning that the measurements presented in their paper probably reflect the sizes of the anterior openings of the VC and the FR. Such anterior view of the 3D reconstructions resulted in the distance between the VC and the SPF to be 3.8 ± 1.0 mm in their study [19], different from the results of the study reported here—which was based on axial slices appreciating the fact that the VC and the SPF are not located in the same frontal plane.

Multiple patterns of posterior MS wall pneumatization are described, such as the presence of Sieur (spheno-ethmoido-maxillary) cells, Haller (infraorbital ethmoido-maxillary) cells, Onodi (spheno-ethmoidal) cells reaching the optic canal, the maxillary recess of the sphenoid sinus, the sphenoid recess of the maxillary sinus, etc [7]. Due to the complexity of the analysis, cases with posterior MS wall pneumatization were not analyzed in this study. Future morphometric studies should include these anatomical variations to evaluate their influence on the PPF volume and the distance from the posterior wall of the PPF to the maxilla.

The communications of the PPF enable the inflammatory and neoplastic processes to spread into other viscerocranial spaces and the skull base [5], such as the cavernous sinus (through the FR), the masticator space (through the PMF), the foramen lacerum (through the VC), and the nasal and

Table 4 Pterygopalatine fossa measurements as obtained by different authors

	Berlis et al. [4]	Kim et al. [22]	Chen et al. [6]	Hwang et al. [11]	Bryant et al. [5]	Mohebbi et al. [24]	Acar et al. [1]
Sample size	60	90	1	98	11	100	250
Study method	CT[a]	CT	CT + thin transverse sections	3D CT	3D CT	CT	CT
Transverse diameter of VC[b] (mm)							
Anterior	–	1.8	3.25	2.4 ± 0.7	–	–	1.9 ± 0.6
Central	–	–	2.25	–	–	–	1.0 ± 0.4
Posterior	–	1.2	–	–	–	–	1.6 ± 0.5
Transverse diameter of FR[c] (mm)—level unknown	3.11 ± 0.78	3.0	2.5	2.8 ± 0.5	–	–	–
Transverse diameter of SPF[d] (mm)	–	–	3.9	–	–	–	3.9 ± 0.8
Direct FR–VC distance (mm)	–	rt[e]: 6.3 left[f]: 5.5	–	–	5.09 ± 1.84	rt: 8.16 ± 2.27 left: 9.20 ± 2.15	8.1 ± 2.3
Direct FR—midline distance (mm)	–	–	–	–	–	rt: 19.00 ± 2.07 left: 19.34 ± 2.17	–

[a]Computed tomography

[b]Vidian canal

[c]Foramen rotundum

[d]Sphenopalatine foramen

[e]Right

[f]Left

oral cavities (through the SPF and the GPC) [9]. The morphology of the PPF depends on the degree of pneumatization of the surrounding bones [24, 30]. Surgical interventions in the PPF are carried out to treat various benign and malignant tumors [10], inflammatory pseudotumors [33], trigeminal neuralgia [18], and autonomic head and neck disorders [21]. Endonasal endoscopic approach represents a reliable alternative to the open surgical approach (craniotomy or maxillary osteotomy) with a reduced morbidity [2, 20, 35, 37] and a superior cosmetic result [13]. Application of a vasoconstrictive agent and a local anesthetic in the PPF facilitates paranasal sinus surgery, improving the visualization of the operative field by reducing intraoperative bleeding [3, 36]. The PPF is accessed endoscopically through the SPF [17, 23] and the posterior wall of the MS [11], with an optional inferior turbinectomy [2]. The key landmarks in the transpterygoid approach to the skull base are the SPF, the VC, and the FR [14, 16, 25]. The study presented herein showed a specific approach to the measurement of the FR and the VC transverse diameter: measuring the diameters in a plane parallel to the posterior PPF wall, and not perpendicular to the axes of those communications. This approach is an attempt to respect the angle of the FR and the VC to the posterior wall of the PPF. These results illustrating the area of the PPF posterior wall engaged by the FR and the VC may improve the orientation of the endoscopic surgeons approaching the posterior wall of the PPF.

Modern high-resolution CT enables adequate morphometric measurement of the cranial canals and foramina, presuming that they are perpendicular to the scan axis [4]. 3D skeletal analysis is a relatively expensive and technically demanding procedure that takes a substantial amount of time to complete, with a certain degree of signal noise interfering with the image analysis. These factors limit its use in common clinical practice [34]. Nevertheless, CT imaging and 3D CT evaluation are necessary for the management of diseases affecting the PPF, due to the possibility of individual variations in the dimensions of the osteological elements. This paper contains several new descriptions of the PPF (such as the angle between the SPF and the VC, a new aspect in the understanding of the FR, and the distance between the posterior wall of the MS to the VC and the FR), which might prove useful in the comprehension of the anatomy of the PPF. In addition, the predictive value of VC length in the analysis of VC types can be of use in the endoscopic approach to the sphenoid sinus and the VC. A conclusion is reached that the VCs protruding into the sphenoid sinus are usually longer than the VCs embedded in the pterygoid process—emphasizing the feasibility of the transsphenoidal approach to the type 3 VC.

Author contributions AV-B: data analysis, manuscript writing, and editing; BV: data collection and manuscript writing; MA: data collection and analysis; NV: manuscript writing; NP: manuscript writing; MR: data analysis and manuscript editing.

Compliance with ethical standards

Conflict of interest The authors declare that they have no conflict of interest.

References

1. Acar G, Cicekcibasi AE, Cukurova I, Ozen KE, Seker M, Guler I (2017) The anatomic analysis of the vidian canal and the surrounding structures concerning vidian neurectomy using computed tomography scans. Braz J Otorhinolaryngol S1808-8694(17):30215-X. https://doi.org/10.1016/j.bjorl.2017.11.008
2. Alfieri A, Jho HD, Schettino R, Tschabitscher M (2003) Endoscopic endonasal approach to the pterygopalatine fossa: anatomic study. Neurosurgery 52:374–380
3. Aoun G, Nasseh I, Sokhn S (2016) Radio-anatomical study of the greater palatine canal and the pterygopalatine fossa in a Lebanese population: a consideration for maxillary nerve block. J Clin Imaging Sci 6:35
4. Berlis A, Putz R, Schumacher M (1992) Direct and CT measurements of canals and foramina of the skull base. Br J Radiol 65(776):653–661. https://doi.org/10.1259/0007-1285-65-776-653
5. Bryant L, Goodmurphy CW, Han JK (2014) Endoscopic and three-dimensional radiographic imaging of the pterygopalatine and infratemporal fossae: improving surgical landmarks. Ann Otol Rhinol Laryngol 123(2):111–116. https://doi.org/10.1177/000348941452370
6. Chen CC, Chen ZX, Yang XD, Zheng JW, Li ZP, Huang F, Kong FZ, Zhang C (2010) Comparative research of the thin transverse sectional anatomy and the multislice spiral CT on the pterygopalatine fossa. Turk Neurosurg 20(2):151–158. https://doi.org/10.5137/1019-5149.JTN.2732-09.0
7. Craiu C, Rusu MC, Hostiuc S, Sandulescu M, Derjac-Arama AI (2017) Anatomic variation in the pterygopalatine angle of the maxillary sinus and the maxillary bulla. Anat Sci Int 92:98–106. https://doi.org/10.1007/s12565-015-0320-z8.
8. Daniels DL, Mark LP, Ulmer JL, Mafee MF, McDaniel J, Shah NC, Erickson S, Sether LA, Jaradeh SS (1998) Osseous anatomy of the pterygopalatine fossa. AJNR Am J Neuroradiol 19(8):1423–1432
9. Daniels DL, Rauschning W, Lovas J, Williams AL, Haughton VM (1983) Pterygopalatine fossa: computed tomographic studies. Radiology 149:511–516. https://doi.org/10.1148/radiology.149.2.6622697
10. Derinkuyu BE, Boyunaga O, Oztunali C, Alimli AG, Ucar M (2017) Pterygopalatine fossa: not a mystery! Can Assoc Radiol J 68(2):122–130. https://doi.org/10.1016/j.carj.2016.08.001
11. Elhadi AM, Zaidi HA, Yagmurlu K, Ahmed S, Rhoton AL Jr, Nakaji P, Preul MC, Little AS (2016) Infraorbital nerve: a surgically relevant landmark for the pterygopalatine fossa, cavernous sinus, and anterolateral skull base in endoscopic transmaxillary approaches. J Neurosurg 125(6):1460–1468. https://doi.org/10.3171/2015.9.JNS151099
12. Erdogan N, Unur E, Baykara M (2003) CT anatomy of the pterygopalatine fossa and its communications: a pictorial review. Comput Med Imaging Graph 27(6):481–487
13. Fahmy CE, Carrau R, Kirsch C, Meeks D, de Lara D, Solares A, Otto BA, Prevedello DM (2014) Volumetric analysis of endoscopic and traditional surgical approaches to the infratemporal

fossa. Laryngoscope 124:1091–1096. https://doi.org/10.1002/lary.24428
14. Falcon RT, Rivera-Serrano CM, Miranda JF, Prevedello DM, Snyderman CH, Kassam AB, Carrau RL (2011) Endoscopic endonasal dissection of the infratemporal fossa: anatomic relationships and importance of Eustachian tube in endoscopic skull base surgery. Laryngoscope 121:31–41. https://doi.org/10.1002/lary.21341
15. Fortes FSG, Sennes LU, Carrau RL, Brito R, Ribas GC, Yasuda A, Rodrigues AJ Jr, Snyderman CH, Kassam AB (2008) Endoscopic anatomy of the pterygopalatine fossa and the transpterygoid approach: development of surgical instruction model. Laryngoscope. 118:44–49. https://doi.org/10.1097/MLG.0b013e318155a492
16. Grewal SS, Kurbanov A, Anaizi A, Keller JT, Theodosopulous PV, Zimmer LA (2014) Endoscopic endonasal approach to the maxillary strut: anatomical review and case series. Laryngoscope 124:1739–1743. https://doi.org/10.1002/lary.24528
17. Gu Y, Yu Y, Zhang X, Hu F, Wang X, Xu W, Xie T (2015) Endoscopic endonasal transmaxillary transpterygoid approach to Meckel cave: anatomical study and preliminary clinical results. J Neurol Surg A Cent Eur Neurosurg 76(3):205–210. https://doi.org/10.1055/s-0034-1389092
18. Guo J, Huang D, Chen S, Zhu S, Rong Q (2015) Treatment of a subtype of trigeminal neuralgia with descending palatine neurotomy in the pterygopalatine fossa via the greater palatine foramen—pterygopalatine canal approach. J Craniomaxillofac Surg 43:97–101. https://doi.org/10.1016/j.jcms.2014.10.016
19. Hwang SH, Joo YH, Seo JH, Kim SW, Cho JH, Kang JM (2011) Three-dimensional computed tomography analysis to help define an endoscopic endonasal approach of the pterygopalatine fossa. Am J Rhinol Allergy 25:346–350. https://doi.org/10.2500/ajra.2011.25.363
20. Kantola VE, McGarry GW, Rea PM (2013) Endonasal, transmaxillary, transpterygoid approach to the foramen ovale: radio-anatomical study of surgical feasibility. J Laryngol Otol 127:1093–1102. https://doi.org/10.1017/S0022215113002338
21. Khonsary SA, Ma Q, Villablanca P, Emerson J, Malkasian D (2013) Clinical functional anatomy of the pterygopalatine ganglion, cephalgia and related dysautonomias: a review. Surg Neurol Int 4:S422–S428. https://doi.org/10.4103/2152-7806.121628
22. Kim HS, Kim DI, Chung IH (1996) High-resolution CT of the pterygopalatine fossa and its communications. Neuroradiology 38(1):S120–S126
23. Li J, Xu X, Wang J, Jing X, Guo Q, Qiu Y (2009) Endoscopic study for the pterygopalatine fossa anatomy: via the middle nasal meatus—sphenopalatine foramen approach. J Craniofac Surg 20(3):944–947. https://doi.org/10.1097/SCS.0b013e3181a2d9c8
24. Mohebbi A, Rajaeih S, Safdarian M, Omidian P (2017) The sphenoid sinus, foramen rotundum and vidian canal: a radiological study of anatomical relationships. Braz J Otorhinolaryngol 83(4):381–387. https://doi.org/10.1016/j.bjorl.2016.04.013
25. Oyama K, Tahara S, Hirohata T, Ishii Y, Prevedello DM, Carrau RL. Froelich S, Teramoto A, Morita A, Matsuno A (2017) Surgical anatomy for the endoscopic endonasal approach to the ventrolateral skull base. Neurol Med Chir (Tokyo) 57:534–541. https://doi.org/10.2176/nmc.ra.2017-0039
26. Pinheiro-Neto CD1, Fernandez-Miranda JC, Rivera-Serrano CM, Paluzzi A, Snyderman CH, Gardner PA, Sennes LU (2011) Endoscopic anatomy of the palatovaginal canal (palatosphenoidal canal): a landmark for dissection of the vidian nerve during endonasal transpterygoid approaches. Laryngoscope 122(1):6–12. https://doi.org/10.1002/lary.21808
27. Reymond J, Charuta A, Wysocki J (2005) The morphology and morphometry of the foramina of the greater wing of the human sphenoid bone. Folia Morphol 64(3):188–193
28. Rusu MC (2011) Doubled foramen rotundum and maxillary nerve fenestration. Anat Sci Int 33:723–772. https://doi.org/10.1007/s00276-011-0810-1
29. Rusu MC (2010) Microanatomy of the neural scaffold of the pterygopalatine fossa in humans: trigeminovascular projections and trigeminal-autonomic plexuses. Folia Morphol 69(2):84–91
30. Rusu MC, Didilescu AC, Jianu AM, Paduraru D (2013) 3D CBCT anatomy of the pterygopalatine fossa. Surg Radiol Anat 35:143–159. https://doi.org/10.1007/s00276-012-1009-9
31. Rusu MC, Pop F, Curca GC, Podoleanu L, Voinea LM (2009) The pterygopalatine ganglion in humans: a morphological study. Ann Anat 191:196–202. https://doi.org/10.1016/j.aanat.2008.09.008
32. Sharma NA, Garud RS (2011) Morphometric evaluation and a report on the aberrations of the foramina in the intermediate region of the human cranial base: a study of an indian population. Eur J Anat 15(3):140–149
33. Tashi S, Purohit BS, Becker M, Mundada P (2016) The pterygopalatine fossa: imaging anatomy, communications, and pathology revisited. Insights Imaging 2016 7(4):589–599. https://doi.org/10.1007/s13244-016-0498-1
34. Tomaszewska IM, Kmiotek EK, Pena IZ, Sredniawa M, Czyzowska K, Chrzan R, Nowakowski M, Walocha JA (2015) Computed tomography morphometric analysis of the greater palatine canal: a study of 1500 head CT scans and a systematic review of literature. Anat Sci Int 90(4):287–297. https://doi.org/10.1007/s12565-014-0263-9
35. Uehara M, Tominaga K, Asahina I (2013) Surgical approach to the pterygopalatine fossa—comparison between anterior approach and lateral approach. J Craniofac Surg 24:536–539. https://doi.org/10.1097/SCS.0b013e3182646b44
36. Wormald PJ, Athanasiadis T, Rees G, Robinson S (2005) An evaluation of effect of pterygopalatine fossa injection with local anesthetic and adrenalin in the control of nasal bleeding during endoscopic sinus surgery. Am J Rhinol 19(3):288–292
37. Xu F, Sun X, Hu L, Wang J, Wang D, Pasic TR, Kern RC (2011) Endoscopic surgical treatment of neurogenic tumor in pteryopalatine and infratemporal fossae via extended medial maxillectomy. Acta Otolaryngol 131:161–165. https://doi.org/10.3109/00016489.2010.522594